Scattering by a Dielectric Obstacle in a Rectangular Waveguide

Jawad Abdulnour and Louis Marchildon

Abstract— **A method for the computation of S-parameters associated with a rectangular waveguide with a rectangular or cylindrical obstacle of arbitrary complex scalar permittivity is presented. The method uses modal analysis and integral relationships to connect appropriate components of the field. In this way, convergence is achieved faster than by point-matching techniques. Our method is well adapted to resonance problems, as illustrated by comparison with both theoretical and experimental results.**

I. Introduction

THE scattering of electromagnetic waves by a dielectric obstacle in a rectangular waveguide has been the subject of ongoing research for more than 50 years. To this day, most of the work has focused on the case where the sample's properties are uniform in one of the transverse directions of the guide. This makes the problem essentially two-dimensional. Variational methods for this problem were developed by Schwinger and Saxon [1], and applied by Marcuvitz [2] to a cylinder whose diameter is small with respect to the wavelength.

A number of authors have gone further and tried to overcome limitations of earlier work. Wexler [3] has given a modal analysis of waveguide discontinuities which is not restricted to small samples. Modal analysis, in conjunction with point-matching techniques, was also applied by Nielsen [4] and Sahalos and Vafiadis [5] to cylindrical samples. Leviatan and Sheaffer [6] have used a moment method that simulates the field by a distribution of fictitious currents. Their formalism essentially applies to any two-dimensional geometry. Such is the case also with finite- and/or boundary-element methods, for instance those of Ise and Koshiba [7] and Wu *et al.* [8]. Araneta *et al.* [9] have developed a higher order variational method for a cylindrical sample.

These developments have all improved significantly on earlier work. Each one is characterized by a wider or narrower range of applicability, and more or less economical use of computer resources. Discrepancies remain, however, among results obtained by different methods, particularly near a resonance.

The purpose of this paper is to develop a formalism, based on modal analysis, that can handle cylindrical as well as rectangular samples. The method, instead of using the point-matching techniques of [4] and [5], pushes the analytical treatment one step further. Where it is applicable, it provides a reliable, rapidly converging algorithm for the determination of S-parameters.

Manuscript received April 2, 1992; revised February 17, 1993.

The authors are with the Departement de Physique, Universite du Quebec, Trois-Rivieres, Canada. J. Abdulnour is presently at POLY-GRAMES, Departement de Genie Electrique, Ecole Polytechnique, Montreal, Canada.

IEEE Log Number 9212725.

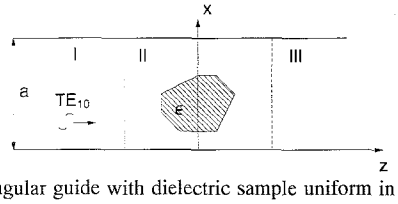

Fig. 1. Rectangular guide with dielectric sample uniform in the y direction.

Section II is devoted to the statement of the problem and modal analysis. Sections III and IV consider the rectangular and cylindrical geometries, respectively. Results are shown in Section V and compared with existing literature. We conclude in Section VI.

II. Modal Formulation

We consider a rectangular waveguide, with z and xy the longitudinal and transverse directions, respectively. A dielectric sample, whose cross section and permittivity are uniform in the y direction, is contained in the guide. The situation is illustrated in Fig. 1. A TE_{10} wave, of unit amplitude, is incident from the left. In this essentially two-dimensional geometry, the only nonvanishing component of the reflected and transmitted electric field is E_y.

Only TE_{m0} modes are produced by the scattering process. As usual, we assume that the frequency of operation is between the cutoffs for the TE_{10} and TE_{20} modes. Far from the sample, then, only the TE_{10} mode survives. The amplitudes of the reflected and transmitted TE_{10} waves, related to the S-parameters of the two-port system, are what we want to determine.

The interior of the guide, as shown in Fig. 1, is divided into three regions. The sample is entirely contained in region II. Boundaries can be chosen in a number of ways, depending on the sample's geometry. Region I extends to the left, and region III to the right of the sample. We have vacuum permittivity and permeability in these regions.

In the configuration shown in Fig. 1, nonvanishing components of the electromagnetic field are E_y, H_x, and H_z. In region I, they are given by a superposition of the incoming TE_{10} and reflected TE_{m0} waves. With a common factor $e^{j\omega t}$removed, we have

$$E_y^{\mathrm{I}} = \phi_1 e^{-\gamma_1 z} + \sum_{m=1}^{\infty} R_m \phi_m e^{\gamma_m z}$$

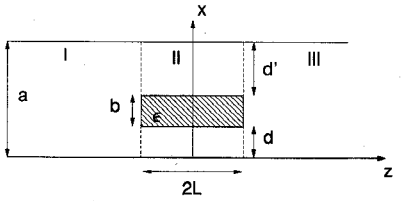

Fig. 2. Rectangular sample with length $2L$ and width b.

$$H_x^{\mathrm{I}} = \frac{j}{\omega\mu_0}\left[\gamma_1\phi_1 e^{-\gamma_1 z} - \sum_{m=1}^{\infty}\gamma_m R_m \phi_m e^{\gamma_m z}\right]$$
$$H_z^{\mathrm{I}} = \frac{j}{\omega\mu_0}\left[\phi_1' e^{-\gamma_1 z} + \sum_{m=1}^{\infty} R_m \phi_m' e^{\gamma_m z}\right]. \quad (1)$$

Here

$$\gamma_1 = j\left[\omega^2\mu_0\varepsilon_0 - \left(\frac{\pi}{a}\right)^2\right]^{1/2} \quad (2)$$

and, for $m \neq 1$,

$$\gamma_m = \left[\left(\frac{m\pi}{a}\right)^2 - \omega^2\mu_0\varepsilon_0\right]^{1/2}. \quad (3)$$

The symbol ϕ_m denotes a normalized trigonometric function which, when the origin of the x axis coincides with the lower conducting wall, is given by

$$\phi_m(x) = \sqrt{\frac{2}{a}}\sin\left(\frac{m\pi x}{a}\right). \quad (4)$$

We have $\phi_m' = \partial\phi_m/\partial x$, and the constant R_m is the amplitude of the reflected TE_{m0} wave.

In region III, the fields are given by a superposition of transmitted TE_{m0} waves. We have

$$E_y^{\mathrm{III}} = \sum_{m=1}^{\infty} T_m \phi_m e^{-\gamma_m z}$$
$$H_x^{\mathrm{III}} = \frac{j}{\omega\mu_0}\sum_{m=1}^{\infty}\gamma_m T_m \phi_m e^{-\gamma_m z}$$
$$H_z^{\mathrm{III}} = \frac{j}{\omega\mu_0}\sum_{m=1}^{\infty} T_m \phi_m' e^{-\gamma_m z}. \quad (5)$$

Here T_m are the transmitted wave amplitudes.

The sample permittivity is, in general, a complex number, as well as the coefficients R_m and T_m. To determine them, we write down, depending on the geometry, appropriate expressions for the fields in region II. The fields are then connected on the boundaries between regions I and II, and between regions II and III. Rather than by point-matching, the connection is effected here by an integral method. This yields values for R_m and T_m and, in particular, for R_1 and T_1.

III. Rectangular Sample

The rectangular geometry is shown in Fig. 2. The sample has complex permittivity ε (and permeability μ_0). It has length $2L$, width b, and is a distance d away from one of the conducting walls. The distance from the other wall is $d' = a - b - d$, where a is the width of the guide (in the x direction). Coordinate axes are defined as shown.

The fields in region II can be written as

$$E_y^{\mathrm{II}} = \sum_{n=1}^{\infty} A_n \psi_n e^{-\Gamma_n z} + \sum_{n=1}^{\infty} B_n \psi_n e^{\Gamma_n z}$$
$$H_x^{\mathrm{II}} = \frac{j}{\omega\mu_0}\left[\sum_{n=1}^{\infty} A_n\Gamma_n\psi_n e^{-\Gamma_n z} - \sum_{n=1}^{\infty} B_n\Gamma_n\psi_n e^{\Gamma_n z}\right]$$
$$H_z^{\mathrm{II}} = \frac{j}{\omega\mu_0}\left[\sum_{n=1}^{\infty} A_n\psi_n' e^{-\Gamma_n z} + \sum_{n=1}^{\infty} B_n\psi_n' e^{\Gamma_n z}\right]. \quad (6)$$

Here A_n and B_n are complex constants. ψ_n are the transverse mode functions, and $\psi_n' = \partial\psi_n/\partial x$.

The TE_{n0} transverse mode functions are given by

$$\psi_n(x) = \begin{cases} f_{1n}\sin(\chi_{1n}x), \\ \quad \text{if } 0 < x < d \\ f_{2n}\sin(\chi_{2n}x) + g_{2n}\cos(\chi_{2n}x), \\ \quad \text{if } d < x < d+b \\ f_{3n}\sin[\chi_{1n}(a-x)], \\ \quad \text{if } d+b < x < a. \end{cases} \quad (7)$$

Here f_{1n}, f_{2n}, g_{2n}, and f_{3n} are constants given by

$$f_{2n} = \chi_{1n}\cos(\chi_{1n}d)\cos(\chi_{2n}d) + \chi_{2n}\sin(\chi_{1n}d)\sin(\chi_{2n}d)$$
$$g_{2n} = -\chi_{1n}\cos(\chi_{1n}d)\sin(\chi_{2n}d) + \chi_{2n}\sin(\chi_{1n}d)\cos(\chi_{2n}d)$$
$$f_{1n} = \frac{\chi_{2n}}{\chi_{1n}}\left[\frac{\cos(\chi_{2n}d)}{\cos(\chi_{1n}d)}f_{2n} - \frac{\sin(\chi_{2n}d)}{\cos(\chi_{1n}d)}g_{2n}\right]$$
$$f_{3n} = \frac{\chi_{2n}}{\chi_{1n}}\left[-\frac{\cos[\chi_{2n}(d+b)]}{\cos(\chi_{1n}d')}f_{2n} + \frac{\sin[\chi_{2n}(d+b)]}{\cos(\chi_{1n}d')}g_{2n}\right]. \quad (8)$$

We have

$$\chi_{1n} = \left[\omega^2\mu_0\varepsilon_0 + \Gamma_n^2\right]^{1/2}$$
$$\chi_{2n} = \left[\omega^2\mu_0\varepsilon + \Gamma_n^2\right]^{1/2}, \quad (9)$$

where Γ_n, the propagation constants, are calculated from the characteristic equation

$$(\chi_{1n})^2\tan(\chi_{2n}b) - (\chi_{2n})^2\tan(\chi_{2n}b)\tan(\chi_{1n}d)\tan\cdot(\chi_{1n}d') + (\chi_{1n})(\chi_{2n})\{\tan(\chi_{1n}d) + \tan(\chi_{1n}d')\} = 0. \quad (10)$$

Equations (8) and (10) considerably simplify in the special cases where $d = 0$ (sample adjacent to wall) or $d = d'$ (sample midway between walls).

The fields must now be connected on the boundary between regions I and II ($z = -L$) and on the boundary between regions II and III ($z = L$). This can be done by point matching, that is, by equating corresponding field components at selected points on boundaries, and solving the resulting linear system for the unknown coefficients. Instead of doing this, however, we will rather use an integral method, akin to the one used in [3] in a somewhat different context. It turns out that this significantly improves convergence or, to put it differently, the accuracy of the S-parameters obtained from a given number of modes.

On the plane $z = -L$, the tangential components E_y and H_x of the fields must be continuous. So we equate $E_y^{\mathrm{I}}(z = -L)$ with $E_y^{\mathrm{II}}(z = -L)$, and similarly with $H_x^{\mathrm{I}}(z = -L)$ and

$H_x^{\mathrm{II}}(z=-L)$. The two resulting equations are then multiplied on each side with ϕ_m, and integrated over x. Making use of the orthogonality of the ϕ_m functions, we get

$$-R_m e^{-\gamma_m L} + \sum_{n=1}^{\infty} A_n e^{\Gamma_n L} P_{mn} + \sum_{n=1}^{\infty} B_n e^{-\Gamma_n L} P_{mn} = \delta_{1m} e^{\gamma_1 L}$$

$$R_m \gamma_m e^{-\gamma_m L} + \sum_{n=1}^{\infty} A_n \Gamma_n e^{\Gamma_n L} P_{mn} - \sum_{n=1}^{\infty} B_n \Gamma_n e^{-\Gamma_n L} P_{mn} = \gamma_1 \delta_{1m} e^{\gamma_1 L}. \quad (11)$$

Here δ_{1m} is the Kronecker delta, and

$$P_{mn} = \int_0^a \phi_m(x)\psi_n(x)\,dx. \quad (12)$$

On the plane $z = L$, we equate E_y^{II} with E_y^{III}, and H_x^{II} with H_x^{III}. Working as before, we get

$$-T_m e^{-\gamma_m L} + \sum_{n=1}^{\infty} A_n e^{-\Gamma_n L} P_{mn} + \sum_{n=1}^{\infty} B_n e^{\Gamma_n L} P_{mn} = 0$$

$$-\gamma_m T_m e^{-\gamma_m L} + \sum_{n=1}^{\infty} A_n \Gamma_n e^{-\Gamma_n L} P_{mn} - \sum_{n=1}^{\infty} B_n \Gamma_n e^{\Gamma_n L} P_{mn} = 0. \quad (13)$$

We now combine the two equations (11) together to eliminate R_m, and similarly with (13) to eliminate T_m. Since $\gamma_1 \delta_{1m} = \gamma_m \delta_{1m}$, the result is

$$\sum_{n=1}^{\infty} A_n \left(1 + \frac{\Gamma_n}{\gamma_m}\right) P_{mn} e^{\Gamma_n L} + \sum_{n=1}^{\infty} B_n \left(1 - \frac{\Gamma_n}{\gamma_m}\right) P_{mn} e^{-\Gamma_n L} = 2\delta_{1m} e^{\gamma_1 L}$$

$$\sum_{n=1}^{\infty} A_n \left(1 - \frac{\Gamma_n}{\gamma_m}\right) P_{mn} e^{-\Gamma_n L} + \sum_{n=1}^{\infty} B_n \left(1 + \frac{\Gamma_n}{\gamma_m}\right) P_{mn} e^{\Gamma_n L} = 0. \quad (14)$$

These equations, when suitably truncated, constitute a finite linear system for A_n and B_n. The constants γ_m are given by (2) and (3), and Γ_m are obtained by solving the characteristic equation (10). This must be done numerically. Conversely, the integrals P_{mn} can be calculated analytically. Once (14) is solved for A_n and B_n, the reflection coefficients R_m and transmission coefficients T_m are obtained from (11) and (13).

The solution of (11) and (13) gives, through (14), the coefficients A_n, B_n, R_m, and T_m if the sample permittivity ε is known. In practical applications, one is often interested in the inverse problem, that is, to find ε if a coefficient (say R_1 or T_1) is known. It is worth noting that (11) and (13) can also be used in that case. The problem is then nonlinear but can be solved, for instance, by the Newton–Raphson method [10].

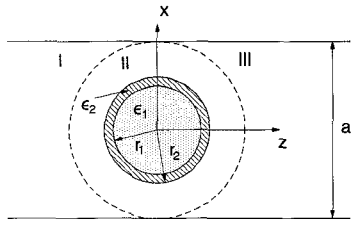

Fig. 3. Concentric dielectric samples of radii r_1 and r_2.

IV. Cylindrical Sample

The cylindrical geometry is shown in Fig. 3. Two concentric dielectric samples, of radii r_1 and r_2 and permittivity ε_1 and ε_2, respectively, are centered midway between the conducting walls. Here it is convenient to choose coordinates so that the origin coincides with the samples' center. The mode functions in regions I and III then become

$$\phi_m(x) = \sqrt{\frac{2}{a}} \sin\left\{\frac{m\pi}{a}\left(x + \frac{a}{2}\right)\right\}. \quad (15)$$

As a consequence of the symmetry about the yz plane, we need keep only odd values of m.

We now address the question of the choice of boundary for region II. Nielsen [4] originally chose the two planes at $z = a/2$ and $z = -a/2$. Sahalos and Vafiadis [5] have chosen a circle of radius $a/2$, centered on the origin. From a fundamental point of view, both choices are objectionable [11]. Nielsen's choice involves using a representation of the fields in terms of cylinder functions [see later, (16)] at distances $r > a/2$, where the series is not known to converge. (See, however, the discussion at the end of [11]). The choice of Sahalos and Vafiadis, on the other hand, involves using modal expansions (1) and (5) at points that do not belong to a uniform cross section of the guide. In Fig. 3, these are points in regions I and III directly above or below samples.

Thus, it may happen that modal expansions (1) and (5) do not provide an exact representation of the fields at those points described earlier. For cylindrical samples of arbitrary radii, the error incurred is difficult to estimate beforehand. There is, however, a well-defined limit in which the error goes to zero, namely, the limit of small radii. In [5], the field matching is done on the broken line shown in Fig. 3. It is easy to see that, as sample radii get smaller and smaller, the arc lengths of the broken lines directly above or below samples go to zero. In this limit then, modal expansions (1) and (5) are correct on essentially all the contours where field matching is done. The outcome is that the choice of Sahalos and Vafiadis is certainly adequate for samples with small radii. We shall see in Section V that it also gives very good results for samples with fairly large radii.

Thus choose the three regions I, II, and III as shown in Fig. 3. In the xz plane, we introduce polar coordinates (r, θ) so that the z axis coincides with $\theta = 0$. In region II, the fields for $r > r_2$ (i.e., outside the samples) are then given by [4]

$$E_y^{\mathrm{II}} = \sum_{n=0}^{\infty} e_n Z_n(kr) \cos(n\theta)$$

$$H_r^{\mathrm{II}} = \frac{-j}{\omega\mu_0}\sum_{n=0}^{\infty}\frac{n}{r}e_n Z_n(kr)\sin(n\theta)$$
$$H_\theta^{\mathrm{II}} = \frac{-j}{\omega\mu_0}\sum_{n=0}^{\infty}e_n k Z_n'(kr)\cos(n\theta)\,. \tag{16}$$

Here e_n are constants, and Z_n is a linear combination of the Bessel and Neumann functions of order n, given by

$$Z_n(kr) = f_n J_n(kr) + Y_n(kr)\,. \tag{17}$$

We have

$$f_n = -\frac{ws_1 - s_2}{ws_3 - s_4}\,, \tag{18}$$

where

$$\begin{aligned}
s_1 &= k_2 Y_n(kr_2)Y_n'(k_2r_2) - kY_n'(kr_2)Y_n(k_2r_2)\\
s_2 &= k_2 Y_n(kr_2)J_n'(k_2r_2) - kY_n'(kr_2)J_n(k_2r_2)\\
s_3 &= k_2 J_n(kr_2)Y_n'(k_2r_2) - kJ_n'(kr_2)Y_n(k_2r_2)\\
s_4 &= k_2 J_n(kr_2)J_n'(k_2r_2) - kJ_n'(kr_2)J_n(k_2r_2)\\
w &= \frac{k_1 J_n(k_2r_1)J_n'(k_1r_1) - k_2 J_n'(k_2r_1)J_n(k_1r_1)}{k_1 Y_n(k_2r_1)J_n'(k_1r_1) - k_2 Y_n'(k_2r_1)J_n(k_1r_1)}\,,
\end{aligned} \tag{19}$$

and

$$\begin{aligned}
k &= \sqrt{\omega^2\mu_0\varepsilon_0}\\
k_1 &= \sqrt{\omega^2\mu_0\varepsilon_1}\\
k_2 &= \sqrt{\omega^2\mu_0\varepsilon_2}\,.
\end{aligned} \tag{20}$$

Here J_n', Y_n', and Z_n' denote the derivatives of J_n, Y_n, and Z_n with respect to their arguments.

In regions I and III, we represent the fields by (1) and (5). Continuity of E_y and H_θ on the boundary between regions I and II yields $(\pi/2 < \theta < 3\pi/2)$ [5]

$$-\sum_{n=0}^{\infty}e_n Z_n\left(\frac{ka}{2}\right)\cos(n\theta) + \sum_{m\,\mathrm{odd}}R_m\phi_m e^{\gamma_m z} = -\phi_1 e^{-\gamma_1 z}$$

$$\sum_{n=0}^{\infty}e_n k Z_n'\left(\frac{ka}{2}\right)\cos(n\theta) - \sum_{m\,\mathrm{odd}}R_m\{\gamma_m\phi_m\cos\theta + \phi_m'\sin\theta\}e^{\gamma_m z} = \{-\gamma_1\phi_1\cos\theta + \phi_1'\sin\theta\}e^{-\gamma_1 z}\,. \tag{21}$$

Similarly, continuity on the boundary between regions II and III yields $(-\pi/2 < \theta < \pi/2)$

$$-\sum_{n=0}^{\infty}e_n Z_n\left(\frac{ka}{2}\right)\cos(n\theta) + \sum_{m\,\mathrm{odd}}T_m\phi_m e^{-\gamma_m z} = 0$$
$$\sum_{n=0}^{\infty}e_n k Z_n'\left(\frac{ka}{2}\right)\cos(n\theta) + \sum_{m\,\mathrm{odd}}T_m\{\gamma_m\phi_m\cos\theta - \phi_m'\sin\theta\}e^{-\gamma_m z} = 0\,. \tag{22}$$

Point-matching techniques were used in [5] to solve the linear system (21) and (22). Here we use an integral method. We multiply (21) and (22) by $\cos(p\theta)$, and integrate on $d\theta$ from $\pi/2$ to $3\pi/2$ in the first case, and from $-\pi/2$ to $\pi/2$ in the second. Making use of the fact that $x = 0$ is a plane of symmetry, we obtain

$$\begin{aligned}
-\sum_{n=0}^{\infty}e_n Z_n\left(\frac{ka}{2}\right)I_{np} + (-1)^p\sum_{m\,\mathrm{odd}}R_m P_{mp}^- &= -(-1)^p P_{1p}^+\\
\sum_{n=0}^{\infty}e_n k Z_n'\left(\frac{ka}{2}\right)I_{np} - \sum_{m\,\mathrm{odd}}R_m Q_{mp}^+ &= -Q_{1p}^-\\
-\sum_{n=0}^{\infty}e_n Z_n\left(\frac{ka}{2}\right)J_{np} + \sum_{m\,\mathrm{odd}}T_m P_{mp}^- &= 0\\
\sum_{n=0}^{\infty}e_n k Z_n'\left(\frac{ka}{2}\right)J_{np} - (-1)^p\sum_{m\,\mathrm{odd}}T_m Q_{mp}^+ &= 0\,,
\end{aligned} \tag{23}$$

where

$$\begin{aligned}
I_{np} &= \int_{\pi/2}^{\pi}\cos(n\theta)\cos(p\theta)\,d\theta\\
J_{np} &= \int_{0}^{\pi/2}\cos(n\theta)\cos(p\theta)\,d\theta\,,
\end{aligned} \tag{24}$$

and

$$\begin{aligned}
P_{mp}^{\pm} &= \int_0^{\pi/2}\phi_m\cos(p\theta)e^{\pm\gamma_m z}\,d\theta\\
Q_{mp}^{\pm} &= \int_{\pi/2}^{\pi}\{\gamma_m\phi_m\cos\theta \pm \phi_m'\sin\theta\}\cos(p\theta)e^{\pm\gamma_m z}\,d\theta\,.
\end{aligned} \tag{25}$$

Here we recall that $z = (a/2)\cos\theta$.

It is easy to see that

$$I_{np} + J_{np} = \begin{cases} 0, & \text{if } n \neq p,\\ \pi/2, & \text{if } n = p \neq 0,\\ \pi, & \text{if } n = p = 0\,. \end{cases} \tag{26}$$

If we add together the first and third of (23) and use (26), we obtain

$$-e_p Z_p\left(\frac{ka}{2}\right)\frac{\pi}{2}[1 + \delta_{0p}] + \sum_{m\,\mathrm{odd}}\{(-1)^p R_m + T_m\}P_{mp}^- = -(-1)^p P_{1p}^+\,. \tag{27}$$

Adding the second and fourth of (23), we similarly obtain

$$e_p k Z_p'\left(\frac{ka}{2}\right)\frac{\pi}{2}[1 + \delta_{0p}] - \sum_{m\,\mathrm{odd}}\{R_m + (-1)^p T_m\}Q_{mp}^+ = -Q_{1p}^-\,. \tag{28}$$

Eliminating e_p from the last two equations, we finally get

$$\sum_{m\,\mathrm{odd}}\left\{\left[(-1)^p k Z_p'\left(\frac{ka}{2}\right)P_{mp}^- - Z_p\left(\frac{ka}{2}\right)Q_{mp}^+\right]R_m + \left[k Z_p'\left(\frac{ka}{2}\right)P_{mp}^- - (-1)^p Z_p\left(\frac{ka}{2}\right)Q_{mp}^+\right]T_m\right\} = -(-1)^p k Z_p'\left(\frac{ka}{2}\right)P_{1p}^+ - Z_p\left(\frac{ka}{2}\right)Q_{1p}^-\,. \tag{29}$$

In (29), everything is known except R_m and T_m. Indeed Z_p and Z_p' can be obtained from (17)–(20), and the $P_{mp}^{\pm}$ and $Q_{mp}^{\pm}$ are computed from (25) by numerical integration. Equation (29), suitably truncated, becomes a finite linear system for R_m and T_m. A related system was also obtained (but not used) in [5]. We note that (29) can also be used for the inverse problem, that is, finding the permittivity of a sample from measured values of a coefficient.

V. Results and Discussion

For nonmagnetic samples with complex permittivity ε, the S-parameters of the two-port systems shown in Figs. 2 and 3 are given in terms of the reflection and transmission coefficients R_1 and T_1 by

$$S_{11} = S_{22} = R_1$$
$$S_{12} = S_{21} = T_1 . \tag{30}$$

Impedances of an equivalent T-circuit are given by

$$Z_a = \frac{2S_{12}}{(1-S_{11})^2 - (S_{12})^2}$$
$$Z_b = \frac{1-(S_{11})^2 + (S_{12})^2 - 2S_{12}}{(1-S_{11})^2 - S_{12}^2} . \tag{31}$$

Computer programs have been devised to evaluate R_1 and T_1 for both the rectangular and cylindrical configurations. In both cases, convergence is tested by increasing the number of modes retained in the linear systems (14) and (29), until results are stable. For ε as high as 150, ten modes are enough to achieve excellent precision.

In the rectangular case, the characteristic equation (10) is solved by bisection combined with the Newton–Raphson method [10]. Explicitly, we set $\varepsilon'' = 0$ and find the first N constants Γ_n by bisection. These results are used as initial values in the Newton–Raphson method, which finds essentially exact values of Γ_n through step-by-step increases of ε''.

In the cylindrical case, $P_{mp}^{\pm}$ and $Q_{mp}^{\pm}$ are computed by the Simpson rule [10]. Fifty intervals are enough to achieve a precision of one part in 10^7.

A. Rectangular Case

Fig. 4(a) and 4(b) shows the amplitude and phase of the reflection and transmission coefficients S_{11} and S_{21}, in the configuration of Fig. 2 with $d = 0$ (sample adjacent to wall). Here ε is real and relatively small. λ is the free-space wavelength.

Fig. 5 shows the amplitude of the reflection coefficient in the configuration of Fig. 2 with $d = d'$ (sample midway between walls). Here ε is real and large. Also shown in Fig. 5 are experimental values of Yoshikado and Taniguchi [12], and a curve they have obtained with the use of an approximate Green's function. The agreement between the experimentally observed resonance and our calculation is striking.

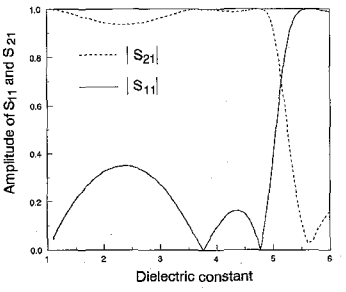

(a)

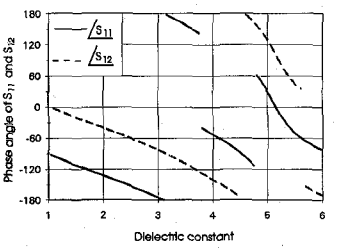

(b)

Fig. 4. S_{11} and S_{21} for a rectangular sample adjacent to wall. $d = 0$, $b = 2L = 0.5a$, $\lambda = 1.4a$. (a) Amplitudes. (b) Phases.

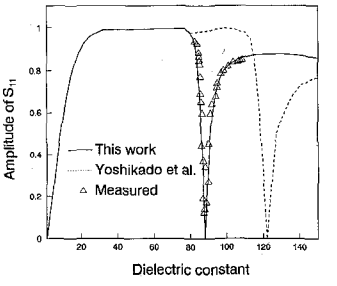

Fig. 5. Amplitude of S_{11} for a rectangular sample midway between walls. $d = d'$, $b = 2L = 0.1a$, $\lambda = 1.4a$.

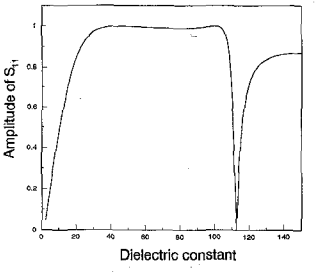

Fig. 6. Amplitude of S_{11} for a lossless cylindrical sample. $r = 0.05a$, $\lambda = 1.4a$.

B. Cylindrical Case

Fig. 6 shows the amplitude of the reflection coefficient in a configuration similar to that of Fig. 3, but for one sample only. The resonance displayed occurs at $\varepsilon = 112.5$, which agrees with results of Sahalos and Vafiadis [5] and Leviatan and Sheaffer [6].

Figs. 7 and 8 show equivalent circuit resistances R_a and R_b and reactances X_a and X_b for a lossy dielectric. Our results disagree with those of Leviatan and Sheaffer [6]. As

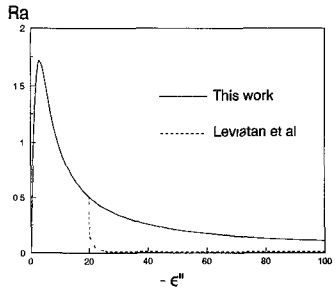

(a)

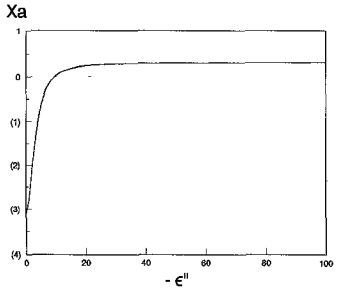

(b)

Fig. 7. Impedance Z_a for a lossy cylindrical sample. $r = 0.05a$, $\lambda = 1.4a$, $\varepsilon' = 4$. (a) Real part. (b) Imaginary part.

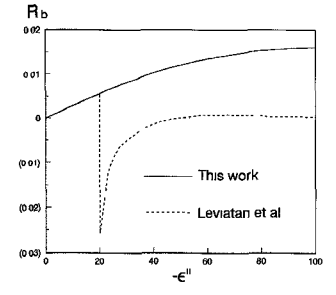

(a)

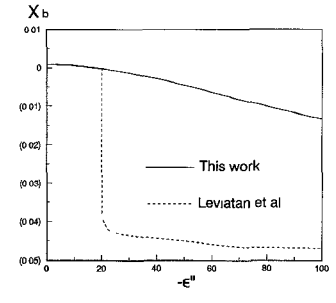

(b)

Fig. 8. Impedance Z_b for the sample of Fig. 7(a) and 7(b).

Table I shows, however, our results agree with those of Ise and Koshiba [7], who have used a combination of finite and boundary elements.

Table II illustrates the convergence of our results. Note that with four modes our results essentially agree with results obtained by Sahalos and Vafiadis [5] with nine modes. This illustrates the rapid convergence of our integral method, compared with point matching.

TABLE I
IMPEDANCES Z_a AND Z_b AND TOTAL POWER REFLECTED AND TRANSMITTED FOR A LOSSY CYLINDRICAL SAMPLE
($r = 0.05a$, $\lambda = 1.4a$, $\varepsilon' = 4$)

	Ise and Koshiba					This work				
- ε''	R_a	X_a	R_b	X_b	P	R_a	X_a	R_b	X_b	P
0	$-3\,10^{-5}$	-3.1872	$-1\,4\cdot10^{-4}$	0.0012	1 0003	$7\,6\,10^{-15}$	-3.1872	$7\,2\,10^{-14}$	0 0009	1.0000
3	1.7096	-1.4775	0.0009	0.0012	0.7563	1.7096	-1 4775	0 0009	0 0009	0.7560
11	0 8677	-0.0044	0.0035	0 0009	0 5295	0 8677	-0.0043	0.0036	0.0006	0 5292
20	0.5012	0.1574	0.0063	0.0001	0.4996	0 5012	0 1573	0 0064	-0 0002	0 4993
120	0 0908	0 2342	0 0183	-0 0180	0 7213	0 0907	0.2342	0.0184	-0.0183	0.7208
1000	0 0247	0 2117	0 0081	-0 0379	0 8933	0 0247	0 2117	0 0082	-0 0382	0 8930
$4\,10^6$	$6\,10^5$	0.1903	-0.0001	-0.0470	1.0002	0.0003	0 1907	0.0001	-0 0470	0 9982

TABLE II
AMPLITUDES OF R_1 AND T_1 COMPUTED WITH 2, 4, 6, AND 9 MODES FOR A CYLINDRICAL SAMPLE
($r = 0.25a$, $\lambda = 1.2732a$)

	2 modes		4 modes		6 modes		9 modes	
ε	|R|	|T|	|R|	|T|	|R|	|T|	|R|	|T|
2	0 2436	0 9699	0 2430	0 9700	0 2430	0.9700	0.2430	0.9700
10	0.1477	0.9890	0 0663	0 9978	0 0661	0 9978	0 0661	0.9978
10	(0.2784)	(0.9527)			(0.0732)	(0 9928)	(0.0668)	(0.9978)
50	0.7565	0.6539	0.7582	0.6519	0 7582	0.6520	0.7582	0 6520

Values in parentheses taken from [5].

We pointed out in Section IV that, strictly speaking, our analysis of cylindrical samples is justified in the limit of small radii. This case is interesting since concentric samples with small radii (e.g., a liquid in a capillary, or a post with coating) may be difficult to analyze with the finite- or boundary-element methods. However, it turns out that our method also gives an excellent approximation even in cases of large radii. We have compared results of our approach with a calculation based on boundary elements, for a cylinder with diameter $0.8a$. For ε as large as 100, numerical values of the reflection and transmission coefficients agree in both calculations on the average to better than 1%.

In closing this section, we should like to point out that (11), (13), and (23) were obtained through integration of the field-matching equations over trigonometric functions. The result is a procedure that converges faster than point matching. It may turn out that weighting functions other than trigonometric give different rates of convergence. It would be interesting to investigate what type of weighting functions provide the fastest rate.

VI. CONCLUSION

We have proposed a largely analytical method for the computation of S-parameters of a rectangular waveguide with rectangular or cylindrical samples. Integral operations are used instead of point matching. Where it is applicable, the method provides a reliable and rapidly converging algorithm. The geometry, although restricted, is one frequently used in applications. Our method can also be used in testing computations with more general geometries.

REFERENCES

[1] J. Schwinger and D. S. Saxon, *Discontinuities in Waveguides.* New York: Gordon and Breach, 1968.
[2] N. Marcuvitz, Ed., *Waveguide Handbook,* MIT Rad. Lab. Ser., vol. 10. New York: McGraw-Hill, 1951.

[3] A. Wexler, "Solution of waveguide discontinuities by modal analysis," *IEEE Trans. Microwave Theory Tech.*, vol. MTT-15, pp. 508–517, 1967.
[4] E. D. Nielsen, "Scattering by a cylindrical post of complex permittivity in a waveguide," *IEEE Trans. Microwave Theory Tech.*, vol. MTT-17, pp. 148–153, 1969.
[5] J. N. Sahalos and E. Vafiadis, "On the narrow-band microwave filter design using a dielectric rod," *IEEE Trans. Microwave Theory Tech.*, vol. MTT-33, pp. 1165–1171, 1985.
[6] Y. Leviatan and G. S. Sheaffer, "Analysis of inductive dielectric posts in rectangular waveguides," *IEEE Trans. Microwave Theory Tech.*, vol. MTT-35, pp. 48–59, 1987.
[7] K. Ise and M. Koshiba, "Numerical analysis of H-plane waveguide junctions by combination of finite and boundary elements." *IEEE Trans. Microwave Theory Tech.*, vol. MTT-36, pp. 1343–1351, 1988.
[8] K. L. Wu, G. Y. Delisle, D. G. Fang, and M. Lecours, "Waveguide discontinuity analysis with a coupled finite-boundary element method," *IEEE Trans. Microwave Theory Tech.*, vol. MTT-37, pp. 993–998, 1989.
[9] J. C. Araneta, M. E. Brodwin, and G. A. Kriegsmann, "High-temperature microwave characterization of dielectric rods," *IEEE Trans. Microwave Theory Tech.*, vol. MTT-32, pp. 1328–1335, 1984.
[10] W. H. Press, B. P. Flannery, S. A. Teukolsky, and W. T. Vetterling, *Numerical Recipes.* Cambridge: Cambridge University Press, 1986.
[11] L. Lewin, "On the inadequacy of discrete mode-matching techniques in some waveguide discontinuity problems," *IEEE Trans. Microwave Theory Tech.*, vol. MTT-18, pp. 364–372, 1970.
[12] S. Yoshikado and I. Taniguchi, "Microwave complex conductivity of a square post in rectangular waveguide," *IEEE Trans. Microwave Theory Tech.*, vol. MTT-37, pp. 984–992, 1989.

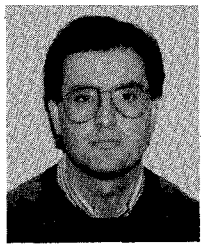

Jawad Abdulnour was born in Beyrouth, Lebanon, in 1960. He completed his undergraduate studies in physics at the Lebanese University in Beyrouth in 1982. He spent several years in France, and then went to the Université du Québec à Trois-Rivières, where he received the M.Sc. degree in physics in 1989, and the Ph.D. degree in energy sciences in 1993.

He is currently working as a Postdoctoral Fellow at Ecole Polytechnique, Montréal.

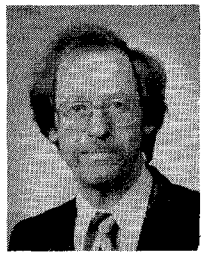

Louis Marchildon was born in Trois-Rivières, Canada, in 1950. He received the B.Sc. and M.Sc. degrees in physics from the Université du Québec à Trois-Rivières in 1972 and 1973, respectively. He obtained the Ph.D. degree in physics from Yale University in 1978.

After two years of postdoctoral work, he held the position of NSERC Research Fellow at the Université du Québec à Trois-Rivières from 1980 to 1985. Since then he has been teaching physics there. He also has research interests in relativity theory.